

Optical Properties of Excitons in Semiconductor Quantum Wells and Microcavities

L.C. ANDREANI

*Istituto Nazionale per la Fisica della Materia and Dipartimento di Fisica 'A. Volta',
Università degli Studi di Pavia, via Bassi 6, I-27100 Pavia, Italy*

A few basic properties of excitons in quantum wells and in semiconductor microcavities are reviewed at an introductory level. The first lecture treats electron-hole and center-of-mass quantization regimes in wide quantum wells, electron-hole and center-of-mass localization in narrow quantum wells, and excitons bound to interface defects: emphasis is given on the behavior of the oscillator strength, which marks clearly the crossover between the various regimes. The second lecture deals with planar microcavities and the strong coupling regime of exciton-radiation interaction, three-dimensional microcavities and the modification of spontaneous emission rate (Purcell effect), and the possibility of obtaining a vacuum-field Rabi splitting for quantum dots in three-dimensional microcavities.

1 Excitons in quantum wells

1.1 Introduction [1-3]

Excitons are electronic excitations of a crystal which go beyond the independent-electron approximation and represent the bound states of an electron-hole pair. Excitons in semiconductors are usually of the shallow, or Wannier-Mott type: i.e., the binding energy is small compared to the band gap and the average electron-hole radius is much larger than the lattice constant. Wannier-Mott excitons are described with good accuracy by a two-particle effective-mass equation in which the kinetic terms contain the effective masses of electron and hole and the Coulomb attraction is screened by the dielectric constant of the crystal. The binding energy of the ground state, or effective Rydberg, is given by $R^* = \mu^* e^4 / 2\epsilon_r^2 \hbar^2$ (where μ^* is the reduced effective mass and ϵ_r the dielectric constant) and is much smaller than the atomic Rydberg due to the small effective mass and large dielectric constant of semiconductors. Each excitonic level has a quadratic dispersion with the total electron-hole mass. Excitonic effects in bulk semiconductors are observable only at low temperature, when the linewidth due to electron-phonon scattering is smaller than the binding energy.

The interaction of excitons with the electromagnetic field is characterized by a dimensionless quantity, the *oscillator strength*, which is defined as follows:

$$f = \frac{2}{m_0 \hbar \omega} \left| \langle \Psi_{\text{exc}} | \mathbf{e} \cdot \sum_i \mathbf{p}_i | \Psi_0 \rangle \right|^2, \quad (1)$$

where Ψ_0 (Ψ_{exc}) is the ground (excitonic) state, \mathbf{p}_i are the electron momentum operators, \mathbf{e} is the polarization vector, m_0 is the free electron mass and ω is the frequency of the transition. The oscillator strength of an exciton associated with an allowed interband transition is nonzero only for s states and decreases as n^{-3} , where n is the principal quantum number. The oscillator strength of a bulk excitonic transition is proportional to the crystal volume, so the quantity of physical significance is the oscillator strength per unit volume, which is related to the absorption coefficient integrated over the transition line (provided polaritonic effects can be neglected) [2].

A *quantum well* is a thin layer of a semiconductor surrounded by thick layers of another semiconductor with a larger band gap. The alignment of the bulk band structures determines the band discontinuity, or *band offset*, between conduction (or valence) band edges. The variation of the band edge from one material to the other gives rise to quantum confinement effects; we consider here only type-I structures, in which electrons and holes are confined in the same material. Electronic states in heterostructures (quantum wells, superlattices, and systems of lower dimensionality like quantum wires and dots) can be treated in a phenomenological yet accurate way by the *envelope-function method* [1]. In this framework, electrons and holes are described by an effective mass equation (possibly a multiband one in the case of band degeneracy) with a confining potential determined by the band offset. A quantum well is characterized by a square-well potential, leading to the particle-in-a-box problem of quantum mechanics. The motion along the growth direction (taken as z) is quantized, but the energy levels have a two-dimensional dispersion $E_n(\mathbf{k}_{\parallel})$ as a function of in-plane wavevector \mathbf{k}_{\parallel} and are called *subbands*.

Excitons in quantum wells are described by the following hamiltonian (E_g is the band gap of the well material and $V_e(z_e)$, $V_h(z_h)$ are square-well confining potentials) [4]:

$$H = E_g - \frac{\hbar^2 \nabla_e^2}{2m_e^*} - \frac{\hbar^2 \nabla_h^2}{2m_h^*} + V_e(z_e) + V_h(z_h) - \frac{e^2}{\epsilon_r |\mathbf{r}_e - \mathbf{r}_h|}. \quad (2)$$

The interplay between quantum confinement and electron-hole attraction gives rise to various physical regimes, which are the subject of this lecture. The oscillator strength of a quantum-well exciton is proportional to the sample surface: only the oscillator strength per unit area has a physical meaning. It can be measured from the *absorption probability* (a dimensionless quantity) integrated over the excitonic peak [2].

In the strict two-dimensional limit (vanishing well width and infinite barrier height) the hamiltonian (2) describes a hydrogenic problem in two dimensions: the binding energy of the ground state is $4R^*$ and the effective Bohr radius a_B is half the bulk value. Starting from a very wide quantum well and reducing the well width L , the binding energy has a monotonic increase from the bulk value R^* to the 2D value $4R^*$ if the barrier heights are taken as infinite [5,6]. However, when the finite band offset is considered, the binding energy reaches a maximum and decreases again towards the three-dimensional value when the well width goes to zero [7]: this is due to the fact that the carrier wavefunctions leak into the barrier material for small well widths. The oscillator strength also has a maximum when the binding energy does.

1.2 Electron-hole versus center-of-mass confinement in wide quantum wells

The increase of the binding energy E_b over the bulk value, due to confinement-induced decrease of the electron-hole separation, leads to more stable exciton states and to much more prominent excitonic effects in absorption and photoluminescence. Several calculations of binding energies, oscillator strengths and absorption spectra of quantum well excitons have been published. Most of them refer to a range of well thicknesses of the order of or smaller than the exciton radius a_B : in this case electron and hole subbands are separately confined and the exciton can be associated with a pair of subbands. This situation is called *strong* (or *electron-hole*) *confinement regime*. An accurate determination of binding energies and oscillator strengths in the strong confinement regime requires the inclusion of additional physical effects like degeneracy of the bulk valence band and mixing of quantum well subbands (the heavy hole-light hole mixing problem [1]), conduction band nonparabolicity, discontinuity of the effective masses and of the dielectric constant between well and barrier materials. When all these effects are taken into account, the calculated values for the ground state binding energy turn out to be strongly increased [8], in particular the maximum binding energy in GaAs/AlGaAs quantum wells can become larger than the two-dimensional value $4R^*$: this has been verified experimentally [9]. Calculating absorption spectra in the continuum requires solving the Schrödinger equation in \mathbf{k} -space [10].

When the well width becomes larger than the exciton radius a different physical regime is reached. This can be seen by comparing the characteristic energies: $E_c = \pi^2 \hbar^2 / (2m^* L^2)$ for quantum confinement, R^* for the Coulomb attraction. When $L \sim a_B$ quantum confinement dominates, electron and hole subbands are separately quantized with quantization energies E_e , E_h and any pair of subbands gives rise to a quasi-2D excitonic series: the energy spectrum is given by $E_{exc} = E_g + E_e + E_h - E_b$. When $L \gg a_B$, on the other hand, the Coulomb interaction dominates and must be diagonalized first, which means that the excitonic center of mass is quantized as a whole in a thin film [11,12]. The quantization width is $L-2D$, where D is a dead-layer thickness. In this *weak* (or *center of mass*) *confinement*

regime the energy spectrum is approximately given by $E_{\text{exc}}=E_g-R^*+\pi^2\gamma^2/(2M(L-2D)^2)$. The two regimes can be distinguished by the energy of photoluminescence peaks.

It is interesting to look at the behavior of the oscillator strength at the crossover from strong to weak confinement. In the electron-hole confinement regime the oscillator strength increases on decreasing well width, due to the reduced separation between electron and hole. On the other hand when the excitonic center of mass is quantized the oscillator strength increases with increasing well width, because it is proportional to the volume occupied by the center of mass. Thus the oscillator strength must have a *minimum* at the crossover from strong to weak confinement, as measured for CdTe/CdZnTe quantum wells [13] and calculated for CuCl quantum wells [14]. Apparently, no systematic investigations of the crossover regime exist for the thoroughly studied GaAs/AlGaAs system. Anyway, it appears that the oscillator strength is a more significant quantity than the binding energy to characterize the different regimes for the excitonic states.

1.3 Electron-hole versus center-of-mass localization in narrow quantum wells

The behavior of exciton states when the well width goes to zero is also interesting and nontrivial. When the well width becomes much smaller than the Bohr radius and the carrier wavefunctions are mostly localized in the barrier region, the single-particle energies are close to the top of the potential well and it is more useful to think of the electronic states of the barrier as the unperturbed ones, while the “quantum well” acts as a localized, nearly δ -like attractive potential. A *localization energy* can be defined by writing the energy of, e.g., electron levels as $E_g^b-E_{\text{loc}}$, where now E_g^b is the band gap of the barrier. The physical behavior of the exciton when the well width goes to zero can be discussed in analogy with the quantum well to thin film crossover. As long as the localization energies of electron and hole remain larger than the exciton binding energy, electrons and holes are separately localized and each pair of electron-hole levels gives rise to an excitonic series: the energy spectrum is given by $E_{\text{exc}}=E_g^b-E_{\text{loc,e}}-E_{\text{loc,h}}-E_b$ and the exciton is still quasi-2D. This can be called a *strong (electron-hole) localization regime*. However when the localization energy becomes smaller than the binding energy (actually that of the barrier material) the Coulomb attraction dominates and the center of mass of the exciton is localized as a whole. In this new regime of *weak (center of mass) localization* the energy spectrum is given by $E_{\text{exc}}=E_g^b-R^*-E_{\text{loc,exc}}$ and the internal exciton wavefunction is that of the bulk barrier material.

Let us look at the behavior of the oscillator strength per unit surface. In the regime of separate electron and hole localization the oscillator strength decreases with decreasing well width, since the carrier wavefunctions become more delocalized in the barriers and the in-plane exciton radius increases towards the 3D value. On the other hand when the exciton is 3D but with a localized center of mass

the oscillator strength is proportional to the localization length: this increases on decreasing the well width, thus the oscillator strength must also increase. This behavior is analog to the so-called “giant oscillator strength” of excitons weakly bound to neutral impurity states in the bulk [15]. As a consequence, the oscillator strength per unit area has again a *minimum* at the crossover from electron-hole to center of mass localization for very narrow quantum wells.

In order to give a quantitative determination of exciton binding energy and oscillator strength in the various physical regimes, a numerical method has been developed [16] in which the exciton states are expanded in a large non-orthogonal basis consisting of products of gaussians in the electron and hole coordinates along the growth direction and exponentials for the relative in-plane motion. Exciton energies and wavefunctions are obtained by calculating hamiltonian and overlap matrix elements and solving a generalized eigenvalue problem. In Fig.1a we show the oscillator strength per unit area in GaAs/Al_{0.15}Ga_{0.85}As quantum wells, as a function of well width in a log scale. The behavior described above can be recognized: the oscillator strength has two minima, in correspondence with the transitions from quasi-2D to 3D behavior for very large or very small thicknesses. The crossover from electron-hole to center of mass confinement in large wells takes place at a well width of about 300 Å, i.e., at $\sim 2.5 a_B$ (the Bohr radius in GaAs is ~ 140 Å). The crossover to center of mass localization in narrow wells occurs for $L \sim 8$ Å. The oscillator strength per unit surface has a local maximum in the quasi-2D regime, but can reach larger values for either very wide or very narrow wells.

The well width at which the oscillator strength has a minimum in narrow quantum wells depends sensitively on the Al concentration in the barriers. For shallow quantum wells ($x \sim 0.01$) the crossover to center of mass localization takes place at $L \sim 100$ Å, as it has been measured in magneto-optical experiments [17]. For $x = 0.35$, on the other hand, the minimum is expected to occur between one and two monolayer thickness. A cathodoluminescence measurement on a sample containing GaAs/Al_{0.35}Ga_{0.65}As quantum wells from one to eight monolayers has been reported in Ref. [18]. The sample is excited from the cleaved edge with the electron beam and the luminescence is collected in the normal direction. The cathodoluminescence signal as a function of electron-beam position shows a well-defined maximal intensity in correspondence to the excitation of each single quantum well: this allows to deduce the oscillator strength of the lowest excitonic transition, which has indeed a minimum around a thickness of three monolayers.

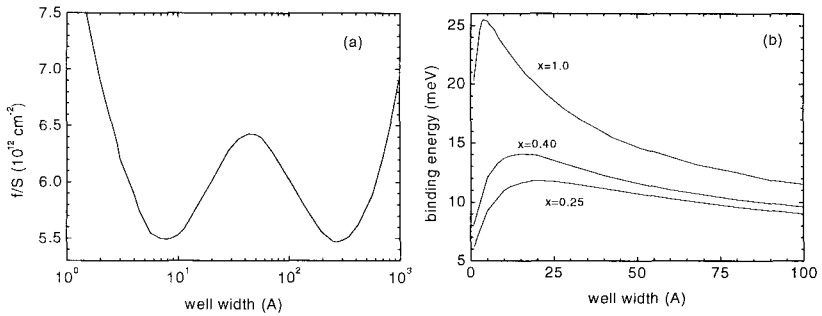


Figure 1. (a) Oscillator strength per unit area of the lowest heavy-hole exciton in GaAs/Al_{0.15}Ga_{0.85}As quantum wells; (b) binding energy of the lowest heavy-hole exciton in GaAs/Al_xGa_{1-x}As quantum wells for different Al concentrations [16].

Calculating the binding energy when the well width goes to zero requires taking into account conduction band nonparabolicity and the variation of effective mass and dielectric constant between well and barriers. The binding energy of the lowest direct exciton (the heavy-hole exciton) in GaAs/Al_xGa_{1-x}As quantum wells is shown in Fig.1b. Note that the limiting values for $L \rightarrow 0$ depend on the Al concentration, since the parameters of the barrier material differ. The maximum binding energy in GaAs/AlAs quantum wells is about 26 meV and it occurs at a few monolayer thickness: this has to be compared with the bulk binding energy ($R^* = 4$ meV in GaAs) and the “2D limit” of $4R^*$. Actually the GaAs/AlAs system becomes type-II for $L < 35 \text{ \AA}$, so the direct exciton is not the lowest one and cannot be observed in photoluminescence: still, the results of Fig.1b show that the variation of the material parameters has an important effect in giving binding energies much larger than the 2D limit. In addition, comparison of Figs. 1a and 1b indicates that the binding energy shows no signature of the crossover from electron-hole to center-of-mass localization: only the oscillator strength allows to clearly mark the crossover.

The limit of ultra-narrow quantum wells is that of monolayer insertions, like an In plane in GaAs or a Ga plane in AlAs. These act as neutral impurity planes with a short-range attractive potential for both electrons and holes. Sub-monolayers of In in GaAs have also been studied: in these systems the monolayer plane is only partially covered with In and is either a random (In,Ga) alloy, or a collection of islands with specific forms and dimensions. Strong radiative properties associated to excitons bound to monolayer and sub-monolayer insertions have been measured [19,20]. The envelope-function approach cannot be justified in these situations, since the layer widths are too narrow to use the bulk parameters of a “well” material.

Tight-binding calculations have shown that single-particle levels bound to the impurity plane exist [21]. A \mathbf{k} -space approach to excitons bound to monolayer insertions has been developed and applied to In impurity planes in GaAs [22]: single-particle levels are calculated with a tight-binding Green function formalism, while exciton states are obtained by solving \mathbf{k} -space equations for the in-plane electron-hole dynamics. The results show that the oscillator strength of excitons bound to one or two monolayers of In in GaAs is larger than in pseudomorphic $\text{In}_x\text{Ga}_{1-x}\text{As}/\text{GaAs}$ quantum wells. Even for a single monolayer the exciton is quasi-2D, i.e., electrons and holes are separately localized.

1.4 Excitons bound to interface defects

GaAs/AlAs quantum wells produced with growth interruption at the interfaces tend to form flat interfaces with large islands corresponding to a thickness variation of one monolayer. Excitons can become localized to these monolayer fluctuations, as shown by local spectroscopy performed with surface masks, which displays a series of very narrow lines in photoluminescence [23]. Each of these lines corresponds to a *single* bound exciton. Monolayer fluctuations with bound excitons represent a nonconventional type of *quantum dot* [24], since they have a fully discretized energy spectrum with no \mathbf{k} -space dispersion (more common quantum dot systems are either nano-crystallites in a glassy matrix, or self-assembled structures like InAs in GaAs produced by strained growth in the Stranski-Krastanow mode). The oscillator strength of the transition from ground to exciton state is now a dimensionless number, like for atomic transitions.

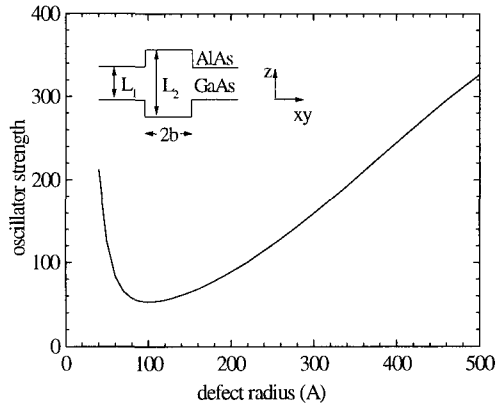
The physics of excitons localized to monolayer fluctuations can be studied by modeling the defect in a quantum well of width L_1 by a disk of radius b in which the well width is $L_2=L_1 + \text{one monolayer}$ (see inset to Fig.2). For narrow quantum wells, the perturbation induced by the defect is much smaller than the quantization energies of electrons and holes. This results in a 2D square-well attractive potential for both carriers, whose strength is given by the difference E_1-E_2 of the energy levels in the quantum wells of width L_1 and L_2 . For defect radii larger than a critical value (typically 30-50 Å) the lowest electron and hole subbands become localized by the lateral potential and the same happens for the exciton.

The limiting cases of a very large or very small defect radius can be understood by arguments similar to those of the previous subsections. For $b \gg a_B$ the carrier wavefunctions are mostly confined within the defect, the quantization energies are smaller than the exciton binding energy and the center of mass motion of the quasi-2D exciton is quantized in a circular potential well. In this regime the oscillator strength is expected to increase with increasing defect radius. For defect radii $b \ll a_B$, instead, the single-particle wavefunctions extend largely in the outer quantum well of width L_1 and the excitonic center of mass is weakly localized. The oscillator strength is proportional to the localization area of the center of mass and

increases with decreasing defect radius, again in analogy to the “giant oscillator strength” [15]. Thus the oscillator strength of excitons bound to monolayer fluctuations must have a *minimum* at a defect radius $b \sim a_B$ and must be large for very small or very large defects.

Binding energies and oscillator strengths of localized excitons have been calculated within the above-described model of a circular defect by expanding the excitonic wavefunctions in the basis of single-particle states with different angular momenta, which in turn are expanded in a large nonorthogonal basis [25,26]. The calculated oscillator strength of the lowest heavy-hole exciton is shown in Fig.2 as a function of defect radius. The behavior expected from the previous considerations is found, with a minimum of the oscillator strength at $b \sim 100 \text{ \AA}$ and an increase for small or large defects. It is interesting to observe that the oscillator strength can reach values up to 200-300: these values are much larger than in self-assembled InAs quantum dots, where the oscillator strength is ~ 10 . In other words, excitons localized to monolayer fluctuations in narrow quantum wells have a stronger coupling with radiation than excitations in InAs dots. The luminescence efficiency depends, of course, on the details of excitation and relaxation processes. Still, the high oscillator strength for localized excitons has important implications when the system is embedded in a three-dimensional microcavity, as we shall see in the next lecture.

Figure 2. Oscillator strength of the lowest heavy-hole exciton localized to a monolayer fluctuation in a GaAs/AlAs quantum well of width $L_1=40 \text{ \AA}$. Inset: model for the attractive defect [25].



2 Radiation-matter interaction in microcavities

Most of semiconductor physics in the last 25 years has been devoted to quantum confined systems like quantum wells, wires, and dots. More recently, progress in growth and processing techniques has allowed to produce structures with confinement of *photonic* states [27]. In a planar microcavity the electromagnetic

field is “quantized” along one direction: this system is the photonic analog of a quantum well. In three-dimensional microcavities, or *photonic dots*, confinement in all spatial directions is achieved. Another possibility for obtaining photon confinement is to employ defects in materials with a photonic band gap. One of the most interesting aspects of the control of photonic states is to study physical phenomena associated with the interaction between confined photonic modes and material excitations. In this lecture I shall discuss a few examples of semiconductor microcavities and of the interaction between excitons and cavity modes.

2.1 Bragg reflector, Fabry-Pérot resonator

In order to have planar solid-state microcavities one needs mirrors with high reflectivity and low losses. In the optical region, multilayer dielectric mirrors, called *Distributed Bragg Reflectors (DBRs)*, are usually employed. A DBR is a periodic repetition of a two-layer unit structure with different refractive indices n_1 , n_2 for the two layers [28,29]. The electromagnetic problem for such a structure is analog to the one-dimensional Kronig-Penney model for electrons. The presence of a refractive index contrast in the medium of period d opens a gap in the photonic dispersion relation $\omega(k)$ when the Bragg condition $k=m\pi/d$ is satisfied, which corresponds to the wavevector k being at the boundary of the Brillouin zones. A *photonic gap* is a forbidden energy region, in which photons cannot propagate: for a finite structure, this means that the reflectivity is large inside the gap and it becomes exponentially close to unity when the number of periods is increased. DBRs have in fact regions of large reflectivity, called *stop bands*, separated by regions called side-bands in which the reflectivity is small and oscillating. For a $\lambda/4$ DBR (i.e., when the thicknesses L_1 , L_2 of two layers satisfy the condition $k_1L_1 = k_2L_2 = \pi/2$ at the operating wavelength) the reflectivity at normal incidence is $R=1-4(n_L/n_H)^{2N}$, where n_L (n_H) is the lower (higher) of the refractive indices and N is the number of periods. The reflectivity is large within a frequency region which depends on the refractive index contrast, and within an angular cone whose width also depends on the contrast: indeed, the center of the stop band has an angular dispersion which (for small contrast and small internal angle θ) goes approximately like $\omega_s(\theta)=\omega_s(0)/\cos\theta$.

A planar Fabry-Pérot microcavity is an epitaxial structure in which a central cavity region of width L_c is surrounded by two mirrors. If the reflection amplitude of the mirrors is assumed to be real and independent of frequency (an approximation which may be valid for metallic, but not for dielectric mirrors) the transmission coefficient is found to have resonances when the Fabry-Pérot condition $k_cL_c=m\pi$ is satisfied: this corresponds to the cavity width being an integer multiple of half wavelengths. The Fabry-Pérot condition is modified for semiconductor microcavities with dielectric mirrors, due to the fact that the reflection amplitude of a DBR is complex and frequency-dependent. The Fabry-Pérot resonance can be viewed as a quasi-bound state of light which is analog to the quantized level of an electron in a

potential well (or, more precisely, to the quasi-bound state corresponding to the tunneling resonance in a double-barrier configuration). The transmission resonance has a Lorentzian lineshape characterized by a frequency ω_m and a linewidth γ_m : the *quality factor* of the Fabry-Pérot mode is defined as $Q_m = \omega_m / \gamma_m$ and is proportional to $(1-R)^{-1}$, where R is the mirror reflectivity.

Like the center of the stop band, the resonance frequency ω_m has an angular dispersion like $\omega_m(\theta) = \omega_m(0) / \cos \theta$ (for small index contrast and internal angle): this can be derived by writing the frequency in terms of wavevector components and noting that the wavevector along the growth direction is discretized by the Fabry-Pérot condition. The dispersion of the Fabry-Pérot mode is sometimes referred to as “heavy photons”, since the optical mode has a quadratic dispersion for small in-plane wavevector and can be characterized by an “effective mass”.

In Fig.3 we see an example of calculated reflectivity for a planar semiconductor microcavity. The reflectance in the case of the cavity alone (Fig.3a) displays the stop band of the DBRs with the narrow Fabry-Pérot resonance at the center. The reflectance for the cavity with embedded quantum wells (Fig.3b) shows the phenomenon of strong-coupling regime of exciton-radiation interaction, to be discussed in the next subsection.

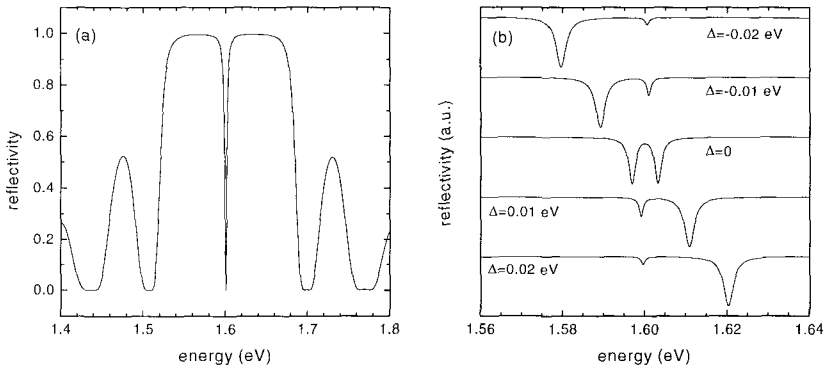


Figure 3. (a) Reflectivity at normal incidence for a $\text{Al}_{0.2}\text{Ga}_{0.8}\text{As}$ λ -cavity with 20 period $\text{Al}_{0.4}\text{Ga}_{0.6}\text{As}/\text{AlAs}$ DBRs; (b) reflectivity of the cavity with five quantum wells at the center, with an exciton resonance at 1.6 eV, for different detunings of the cavity mode (marked on each curve).

Planar microcavities can be employed to modify the emission pattern of a dipole. This effect was demonstrated in Refs. [30,31]. The emitter is a quantum-well exciton: since the quantum well is embedded at the center of the cavity, and the ground-state exciton is a heavy-hole state which is dipole-allowed only for in-plane

polarization, the emitter can be represented by a planar sheet of radiating dipoles placed at the middle of the cavity and oriented in the xy -plane. The experimental (and theoretical) results are as follows. When the exciton frequency ω_{ex} is resonant with the Fabry-Pérot mode at normal incidence, the emission of the dipoles is concentrated in the forward direction. On the other hand, when the exciton resonance is higher than the $\theta=0$ Fabry-Pérot mode the emission pattern is concentrated in a cone at a finite angle, corresponding to the resonance condition $\omega_m(\theta)=\omega_{\text{ex}}$. The change of the emission *pattern* is the basis for the operation of Vertical-Cavity Surface Emitting Lasers (VCSELs). On the other hand the emission *lifetime* is not (or little) modified in a planar microcavity: indeed, the decay rate as a function of angle is found to be enhanced at resonance, suppressed off-resonance, and oscillating when emission is in the side-bands of the dielectric mirrors: the average over all angles gives a decay rate which is close to that in the absence of a microcavity [32]. In order to modify the radiative lifetime three-dimensional photon confinement is needed, as we shall see.

2.2 *Quantum-well excitons in planar microcavities: weak and strong coupling regimes*

A very interesting phenomenon which takes place in planar microcavities with embedded quantum wells is the strong-coupling regime of radiation-matter coupling. This manifests itself as a splitting between coupled exciton-photon modes at resonance, as was first shown in a pioneering paper by Weisbuch et al [33]. The experiment is done by measuring the reflectivity at different positions on the sample surface: since the sample thickness is nonuniform due to inhomogeneous epitaxial growth, the frequency of the Fabry-Pérot mode depends on the position, thus the detuning between the optical mode and the exciton resonance can be changed at will. At zero detuning, two dips are observed in reflectivity with a splitting of a few meV (see Fig. 3b). If the dip positions are plotted as a function of detuning, a clear anticrossing behavior is seen with a minimum separation at resonance. The energy separation at resonance is called *vacuum-field Rabi splitting*: it represents the splitting between mixed modes arising from the interaction between quantum confined excitons in the quantum wells and the Fabry-Pérot mode of the cavity.

The mixed exciton-cavity modes are the analog of exciton-polaritons in bulk semiconductors. Polaritons arise from the interaction between a dipole-active elementary excitation and the electromagnetic field [34,35,2,3]. They can be discussed in a semiclassical framework, which consists of solving Maxwell equations for the electromagnetic field with a constitutive relation between polarization and electric fields which has the resonant form of a Lorentz oscillator. The solutions of Maxwell equations in a cubic medium separate into transverse and longitudinal ones. Transverse (retarded) waves are characterized by the dispersion relation $c^2k^2/\omega^2=\epsilon(\omega)$, while the frequency of longitudinal (instantaneous) waves is given by

the equation $\varepsilon(\omega)=0$. When plotted in terms of $\omega(k)$, transverse waves have two branches which are called *lower* and *upper polariton*. The polariton dispersion is characterized by two energy scales: the longitudinal-transverse splitting ω_{LT} , which corresponds to the splitting between longitudinal exciton and lower polariton at large wavevector and is proportional to the excitonic oscillator strength per unit volume; the splitting between upper and lower polaritons at the crossing point between bare exciton and photon frequencies, which is given as $\omega_c=(\omega_T\omega_{LT}/2)^{1/2}$ (here ω_T is the exciton frequency). The polariton splitting ω_c amounts usually to several meV.

Let us come back to excitons in microcavities and sketch a *linear-dispersion theory of Rabi splitting*. We employ again the Fabry-Pérot condition $k_c L_c = m\pi$, but now impose that the relation $k_c = n(\omega)/c$ contains a strongly dispersive refractive index with a Lorentz oscillator form. After squaring we get a quadratic equation for ω of the form $(\omega - \omega_m)(\omega - \omega_T) = \omega_T \omega_{LT} / 2 \equiv \omega_c^2$, which at resonance leads to an energy splitting $\omega = \omega_T \pm \omega_c$: the Fabry-Pérot condition discretizes the wavevector in the bulk polariton dispersion. In other words, the mixed exciton-cavity modes represent two-dimensional exciton polaritons, which are called *cavity polaritons*.

The above argument is a qualitative one, particularly since it does not take into account damping of the Fabry-Pérot mode (expressed by the linewidth γ_m , which represents the inverse of the escape time of photons) and of the exciton (given by a linewidth γ_{ex} , which may have homogeneous and inhomogeneous contributions). When radiative coupling together with dampings are considered, two regimes can occur: for a radiative coupling smaller than the dampings the exciton-radiation interaction is in a weak coupling regime, which means that the exciton has a radiative decay but with a modified emission pattern; when exciton-light coupling is larger than damping the strong-coupling regime takes place, in which quasi-stationary cavity polaritons are formed and a Rabi splitting occurs. A semiclassical theory of exciton-cavity polaritons requires solving Maxwell equations for the multilayer structure, which can be done in a transfer-matrix formalism [36,37,38]. The complex mixed-mode energies close to resonance are found to be accurately given by a two-oscillator model, in which two states of frequencies $\omega_{ex} - i\gamma_{ex}$ and $\omega_m - i\gamma_m$ are coupled by a matrix element $V = (2\pi e^2 f_{xy} / (\epsilon_r m_0 L_{eff}))^{1/2}$, where f_{xy} is the oscillator strength per unit area of the quantum-well exciton and L_{eff} is an effective cavity length which takes into account penetration of light in the dielectric mirrors. The precise condition for being in strong coupling is $V > |\gamma_{ex} - \gamma_m|/4$; the Rabi splitting at resonance for low damping is $2|V|$.

The dispersion of cavity polaritons can be measured e.g. by angle-resolved reflectivity or photoluminescence [39]. A Rabi splitting has been observed in III-V microcavities even at room temperature. Cavity polaritons are in fact easier to observe than bulk polaritons and have been the subject of a variety of cw and time resolved investigations in the last years [37,40].

2.3 Photonic confinement in three dimensions: the pillar microcavity. Change of spontaneous emission rate (Purcell effect)

Let us turn to systems with three-dimensional photonic confinement. We shall focus on the *cylindrical (or pillar) microcavity* structure: this is obtained from a planar microcavity by etching laterally to form a cylinder of dielectric with radius of the order of a micron (see Fig.4a) . Photonic confinement in such a structure is given by two mechanisms: vertical confinement is provided by the dielectric mirrors of the planar microcavity, while lateral confinement is given by total internal reflection produced by the discontinuity of the average refractive index. Indeed, for III-V microcavities based on GaAs/AlGaAs or InP/InGaAs the refractive indices of the constituent materials are close to each other and of the order of three; an infinite pillar can be viewed as a cylindrical waveguide [41] where the core has the average refractive index of the dielectric and the cladding is air. For a given wavevector k_z along the axis, guided modes exist in the frequency region between ck_z/n_{in} and ck_z/n_{out} , where n_{in} (n_{out}) is the inner (outer) refractive index; these modes have a transverse wavevector which is real in the core region and imaginary in the cladding, i.e., the electric field is oscillating in the core and exponentially decreasing in the outer medium.

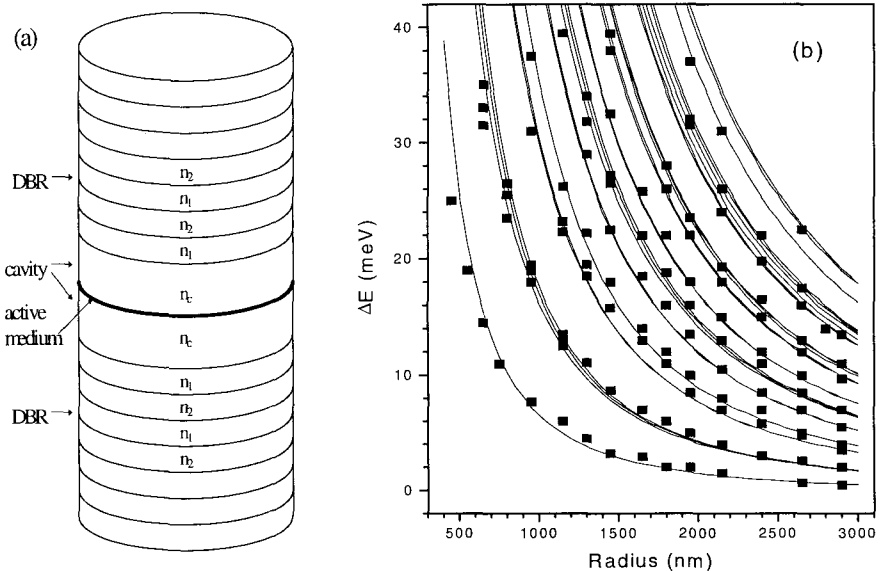


Figure 4. (a) Schematic structure of a pillar microcavity; (b) blue shifts of the lowest energy modes in GaAs/AlGaAs pillar microcavities with respect to the reference planar cavity, as a function of pillar radius. Points: experimental results [42]; solid lines: theoretical results including the energy dependence of the refractive index [43].

While the full problem of calculating the exact photonic modes in a pillar microcavity is a very complex one, a simple approximation for the lowest modes follows from noting that vertical confinement usually dominates and the vertical dynamics can be separated from the lateral dynamics [42]. In this decoupling scheme, the resonance frequencies of the eigenmodes are approximately given as

$$\omega_{lm} = \frac{c}{n_r} \sqrt{\left(\frac{x_{ln}}{a}\right)^2 + \left(\frac{m\pi}{L_c}\right)^2}, \quad (3)$$

where a is the radius of the pillar, L_c is the length of the planar microcavity, and x_{ln} is a zero of a Bessel function of order l : the pillar microcavity acts as a resonant cavity in the optical region, with discretized vertical and transverse wavevector components. The eigenfrequencies (3), or the expressions which result from a more realistic calculations, are those of a *photonic dot*.

The energies of photonic modes in three-dimensional microcavities can be measured from the photoluminescence peaks when the cavity contains a broad-band emitter, since the emission spectrum is concentrated at the energies of cavity modes (a weak continuum emission due to coupling with leaky modes of the waveguide is also present). In the experiment of Ref. [42] the emitter consists in planar array of self-assembled InAs quantum dots placed in a GaAs cavity. In Fig. 4b we show the energies of confined photonic modes as a function of pillar radius. Note that the energy shift on reducing the radius is approximately proportional to $1/a^2$, as follows from Eq. (3) when vertical confinement dominates. Analogous results have been obtained in Ref. [44] with quantum well excitons in rectangular microcavities.

A basic quantum electrodynamic phenomenon which has been recently demonstrated in three-dimensional microcavities is the change of spontaneous emission rate, known as *Purcell effect* [45]. If the emitter has a well-defined frequency and is in resonance with a single cavity mode μ , its emission rate calculated by standard perturbation theory is $\gamma_{SE} = F_\mu \gamma_0$, where γ_0 is the emission rate without the cavity and

$$F_\mu = \frac{3}{4\pi^2} \left(\frac{\lambda}{n_r}\right)^3 \frac{Q_\mu}{V_\mu}, \quad (4)$$

is called the *Purcell factor*. In this formula, $Q_\mu = \omega_\mu / \gamma_\mu$ is the quality factor and $V_\mu = |\alpha_\mu(\mathbf{r})|^2$ is the *mode volume* defined in terms of the the normalized mode function $\alpha_\mu(\mathbf{r})$ of the electric field. The mode volume is calculated at the position of the emitter; it is usually of the order of the cavity volume. The enhancement of the spontaneous emission rate is maximized if the cavity volume is small, the quality factor is large and the emitter is placed at a maximum of the electric field. The

enhanced spontaneous emission in semiconductor microcavities has been recently observed for self-assembled InAs quantum dots in cylindrical microcavities [46].

2.4 Vacuum-field Rabi splitting for quantum dots in three-dimensional microcavities?

The last issue we address in this lecture is the possibility of reaching the strong-coupling regime and observing a vacuum-field Rabi splitting for a single quantum dot in a 3D microcavity [25]. The quantum dot can be modelled as a two-level system with a ground state $|g\rangle$ and an excited state $|e\rangle$; the states of the radiation field for a single mode μ can be denoted as $|n_\mu\rangle$, where n_μ is the number of photons in the mode. The coupling constant $g = \langle e | \mathbf{d} \cdot \mathbf{E} | g \rangle$ of the dipole interaction between the quantum dot transition and the cavity mode is calculated as $g = (\pi e^2 f / (\epsilon_r m_0 V_\mu))^{1/2}$, where f is the oscillator strength of the transition and V_μ is again the mode volume. The quantum Hamiltonian describing the dynamics of the two-level system interacting with the cavity mode is called the Jaynes-Cummings model. Its basis states are the direct product of quantum dot and radiation states: these can be indicated by $|g, n_\mu\rangle$ or $|e, n_\mu\rangle$. At resonance and in the absence of interaction, the ground state is $|g, 0\rangle$, the first excited doublet consists of the degenerate states $|e, 0\rangle$, $|g, 1\rangle$, the second excited doublet consists of $|e, 1\rangle$, $|g, 2\rangle$, etc. The dipole interaction couples the two states of each doublet and produces a splitting $2g(n_\mu + 1)^{1/2}$. The “vacuum-field” Rabi splitting is the one in the lowest doublet, for which one has $n_\mu = 0$ and the splitting is $2\hbar g$.

The above Hamiltonian treatment does not take into account the finite linewidths $\gamma_a, \gamma_{c,\mu}$ of the quantum dot transition and of the cavity mode. Dampings are best treated by a master equation for the density matrix. Within this formalism, the dynamics of the quantum dot-cavity system can be calculated analytically in the case of weak excitation (i.e., when only the ground state and the lowest excited doublet are kept). At resonance, the luminescence spectrum is found to have maxima at complex frequencies given by

$$\Omega_{\pm} = \omega_0 - \frac{i}{4}(\gamma_a + \gamma_c) \pm \sqrt{g^2 - \left(\frac{\gamma_a - \gamma_{c,\mu}}{4}\right)^2}. \quad (5)$$

For $g > |\gamma_a - \gamma_{c,\mu}|/4$ there is a splitting in the real part: this is the vacuum-field Rabi splitting. The condition for being in strong-coupling regime is similar to that for quantum well excitons in planar microcavities, however the physical system has very different behavior since the quantum well exciton is a boson for weak excitation while the quantum dot transition is a fermion. The difference manifests itself in the behavior for increasing excitation intensity: the Rabi splitting of quantum well excitons does not depend on excitation level for weak enough excitation, while the Rabi splitting for a quantum dot transition increases as $(n_\mu + 1)^{1/2}$.

The conditions for having a vacuum-field Rabi splitting require a large coupling constant g , hence a small cavity volume, and small enough linewidths. For InAs quantum dots in micro-pillars, as studied in Ref. [46], the optimal conditions are met for a pillar radius $a=0.5 \mu\text{m}$, when the cavity volume is $V_{\mu}\approx 0.13 (\mu\text{m})^3$, the quality factor is $Q_{\mu}\approx 2 \cdot 10^3$ and the mode width is $\gamma_{c,\mu}=0.6 \text{ meV}$ (the linewidth of the quantum dot transition is about an order of magnitude smaller). The complex energies of Eq. (5) are plotted in Fig. 5 as a function of the oscillator strength. It can be seen that for low oscillator strength there is a splitting in the imaginary part: the upper branch corresponds to the modified quantum dot spontaneous emission rate and gives back the Purcell effect. For high oscillator strength, instead, there is a vacuum-field Rabi splitting in the real part. The strong-coupling regime occurs if the oscillator strength is larger than about 100. For InAs quantum dots the oscillator strength is $f\approx 10$ (this can be deduced e.g. from the measured lifetime $\tau=1.2 \text{ ns}$), thus we conclude that *InAs quantum dots in pillar microcavities are in weak-coupling regime*. Although the quality factor can be improved in different structures like microdisk cavities supporting whispering-gallery modes [47], it seems unlikely that a vacuum-field Rabi splitting can ever be observed for this system.

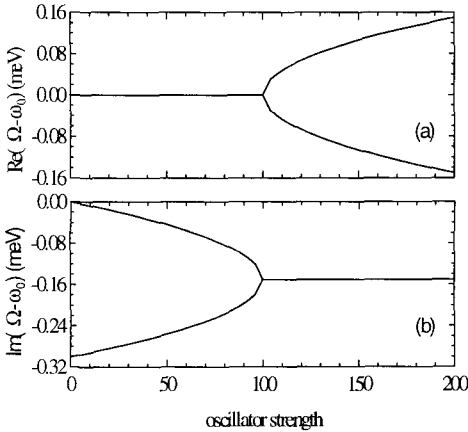


Figure 5. (a) Real and (b) imaginary parts of the energy shifts (Eq. (5)) for the coupling between the lowest mode of a micropillar and the quantum dot transition, as a function of the oscillator strength, for a pillar radius $a=0.5 \mu\text{m}$ and a quality factor $Q_{\mu}=2 \cdot 10^3$ [25].

Thus we need an emitter with a larger oscillator strength. This can be provided by a quantum well exciton localized at interface defects in narrow quantum wells, as discussed in the previous lecture. Indeed, a localized exciton behaves as a zero-dimensional emitter, like in the assumed model of a two-level system, provided the spacing between energy levels remains larger than the cavity mode linewidth: this condition is largely met for defect radii smaller than 500 \AA . The oscillator strength of localized excitons in GaAs/AlAs quantum wells is shown in Fig.2 and its behavior as a function of defect radius was already discussed. We see that the oscillator strength can be much larger than the critical value for having a vacuum-field Rabi splitting,

thus *localized quantum-well excitons embedded in pillar microcavities can be in strong-coupling regime for either small or large defect radius*. Since defects with a large radius can to some extent be controlled by the process of growth interruption, using large defects seems a promising possibility for observing a vacuum-field Rabi splitting with a single three-dimensionally confined emitter in a three-dimensional solid-state microcavity.

3 Acknowledgements

It is a pleasure to acknowledge the collaboration with R.C. Iotti, G. Panzarini, and J.M. Gérard, which led to the results presented in this paper.

References

- [1] Bastard G., *Wave Mechanics applied to Semiconductor Heterostructures* (Les éditions de Physique, Les Ulis Cédex, 1990).
- [2] Andreani L.C., in *Confined Electrons and Photons - New Physics and Devices*, edited by Burstein E. and Weisbuch C. (Plenum, New York, 1995), p.57.
- [3] Yu P.Y. and Cardona M., *Fundamentals of Semiconductors* (Springer, Berlin, 1996).
- [4] Gaussian units are used in this paper. To get formulas in SI units, replace $e^2 \rightarrow e^2/(4\pi\epsilon_0)$, where ϵ_0 is the vacuum permittivity.
- [5] Miller R.C., Kleinman D.A., Tsang W.T. and Gossard A.C., *Phys. Rev. B* **24**, 1134 (1981).
- [6] Bastard G., Mendez E.E., Chang L.L. and Esaki E., *Phys. Rev. B*, **26**, 1974 (1982).
- [7] Greene R.L., Bajaj K.K. and Phelps D.E., *Phys. Rev. B* **29**, 1807 (1984).
- [8] Andreani L.C. and Pasquarello A., *Phys. Rev. B* **42**, 8928 (1990).
- [9] Gurioli M. et al., *Phys. Rev. B* **47**, 15755 (1993).
- [10] Winkler R., *Phys. Rev. B* **51**, 14395 (1995).
- [11] Cho K. and Kawata M., *J. Phys. Soc. Jpn.* **54**, 4431 (1985).
- [12] D'Andrea A. and Del Sole R., *Phys. Rev. B* **41**, 1413 (1990).
- [13] Merle d'Aubigné Y. et al., *J. Cryst. Growth* **101**, 650 (1990).
- [14] Andreani L.C., D'Andrea A. and Del Sole R., *Phys. Lett. A* **168**, 451 (1992).
- [15] Rashba E.I. and Gurgenisvili G.E., *Fiz. Tverd. Tela* **4**, 1029 (1962) [*Sov. Phys.-Solid State* **4**, 759 (1962)].
- [16] Iotti R.C. and Andreani L.C., *Phys. Rev. B* **56**, 3922 (1997).
- [17] Fritze M. et al., *Phys. Rev. Lett.* **76**, 106 (1996).
- [18] Andreani L.C. et al., *Physica E* **2**, 151 (1998).
- [19] Schwabe R. et al., *J. Appl. Phys.* **77**, 6295 (1995).